

## Cone Calorimeter Study of ATH Filled SMC/BMC Formulations

by

Gary C. Rex, J. M. Huber Corp.

### Abstract

NPG-Iso UPE based BMC formulations were compounded with Alumina Trihydrate (ATH) from 150 to 400 phr. Deca-bromo diphenyl ether (DBDE) was compounded with and without ATH. Analysis of mass loss rate, smoke production, and heat release rate plots gives a detailed sequence of events that is consistent with their FR mechanisms.

Initially endothermic decomposition of ATH occurs and controls the rate of pyrolysis in the solid state. Smoke production begins shortly thereafter but is limited to smoldering. Eventually ATH depletion in surface and near surface results in ignition. A rapid rise in HRR culminates in the first HRR peak. HRR decreases and a valley is quickly reached as ATH decomposition renews. The valley is indicative of a period of equilibrium where heat feedback from the combustion phase is balanced by fuel input from the solid phase, i.e., ATH decomposition is controlling the pyrolysis rate. The second and highest HRR peak is reached and corresponds to the complete depletion of ATH. Combustion of the remaining organics creates the peak HRR.

The addition of DBDE was found to reduce the rate of heat release. The reduced HRR in turn reduces feedback of heat into the composite. This has the beneficial effect of reducing the rate of ATH decomposition. Further flattening (reduced intensity) and elongation (longer time) of the MLR, RoSP and HRR curves is observed which is indicative of improving flame retardant (FR) properties.

### Introduction

One of the most widely used flame retardants (FR) on the market today is deca-bromodiphenylether (DBDE). This flame retardant (FR) was to be eliminated from any new EEE (electrical and electronic equipment) by the European Directive, Restriction of Hazardous Substances (RoHS), beginning July 1 2006. An exemp-

tion for DBDE was given on October 15, 2005, citing "at present no need for measures to reduce the risks for consumers beyond which are applied already" [1]. However this exemption was annulled by the European Parliament on April 1, 2008 [2].

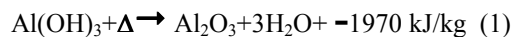
The elimination of DBDE from flame retardant plastics is now a fact in the EU. The rest of the world including the USA is expected to follow suit at some point in the future. Considering the present and future regulatory environment the Composites Industry must develop alternative approaches for achieving acceptable FR performance without the use DBDE. Therefore it is important to understand the ATH FR mechanism as well as the DBDE FR mechanism and the interaction of two in order for acceptable alternative approaches to DBDE be developed.

### Background

#### Flame Retardant Mechanism of ATH

It is important to know that when any polymer burns it first pyrolyzes, releasing low molecular weight flammable gases, which in turn are oxidized by oxygen above the surface of the polymer. This oxidation generates heat, which causes further pyrolysis and so on. Therefore the fire sustains itself. Two important ways flame retardants can act are either in the solid phase as in the case of ATH, or in the gas phase as in the case of halogens such as Br.

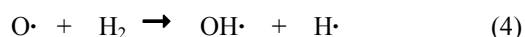
The flame retardant mechanism of alumina trihydrate primarily involves the endothermic decomposition which releases water as shown below:



The decomposition cools the substrate's surface and decreases the rate of pyrolysis in the solid phase. Decreased pyrolysis in turn decreases the rate of volatile organic compounds migrating into the flame zone where they are readily oxidized by oxygen. Secondary effects such as dilution of burnable gases by water vapor, formation of an inert oxide layer, and impeding diffusion of oxygen into the flame zone have also been cited.

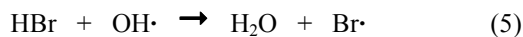
#### Flame Retardant Mechanism of Halogens

Somewhat more complex than the ATH FR mechanism, is the gas phase halogen FR mechanism [3].



Reactions (2) through (4) are extremely important in degrading the high molecular weight pyrolysis products into low molecular weight volatile compounds. The rate of the reaction sequence is largely determined

by the propagation of the high energy OH radical. This radical reacts with hydrobromic acid (in the case of deca-BDE).



The result is the removal of OH radicals from the combustion reaction by HBr as in (5). This cyclic reaction of (5) and (6) is important because OH radicals are responsible for efficient decomposition of the high molecular weight pyrolysis products. This decreases the concentration of volatile, low molecular compounds, the flammable gases in the flame zone, which readily react with oxygen. Therefore the rate of combustion is reduced and becomes more inefficient as witnessed by increased smoke and carbon monoxide [6, 7]

Antimony trioxide is not regarded as flame retardant per se but as a Br synergist. The reaction involves antimony trioxide reacting HBr to produce oxybromide compounds that in turn breakdown into antimony bromide. Antimony bromide is transported into the flame zone where it is thought to interfere, more effectively than HBr, with the cyclic regeneration of the OH radical.

## Experimental

A cone calorimeter model CS-237 [8] by Custom Scientific (ASTM E1354) was used to generate the time to ignition, heat release rate (HRR), mass loss rate (MLR), rate of smoke production (RoSP), and other FR parameters of the samples. The “cone” was run at a heat flux of 50 kW/m<sup>2</sup> in all cases not specified. However in order to determine the intrinsic FR properties the heat flux was varied from 35 kW/m<sup>2</sup> to as high as 75 kW/m<sup>2</sup>. The intrinsic FR properties are those properties that are inherent of the composite, i.e., extrapolated to zero heat flux.

Typical neopentyl glycol – isophthalic (NPG-Iso) unsaturated polyester resin (UPE) was used for all BMC formulations. The polyester resin, initiator, mold release, and fiberglass (15% by weight) were held constant on a phr basis. The level of ATH was varied from 150 phr to 400 phr and the organic resin phase was kept constant at 100 phr. However on a weight % basis this results in the resin phase being varied from a high of 41% to a low 21%. Where added to ATH formulations at 150 phr, 250 phr, and 350 phr formulation, the DBDE/Sb<sub>2</sub>O<sub>3</sub> was kept at a constant phr, 10 phr to 2 phr respectively, and at a constant 5 to 1 ratio in. All of the above is similar to the way formulating is practiced in the industry. In order to compare to ATH at the 250 phr level calcium carbonate was added at the same 250 phr level to serve as a non flame retardant “blank” but whose presence would maintain a resin mass equal to the 250 phr ATH loading for comparison. Exact phrs used in each BMC formulation are shown in Table I.

All liquid components were high sheared first and then followed by the addition of the powder components creating a paste. Lastly a small amount of Mg(OH)<sub>2</sub> was added to prevent separation of the liquid components. The paste was then immediately transferred to a bench top Hobart mixer where 15% by weight fiberglass was incorporated. The BMC was allowed to mature two days before molding. Panels, with dimensions of 12”w x 16”l x 0.100”t, were molded for 2 minutes at ~1,000 psi.

In order to help the reader understand the figures more readily an intuitive fill color code was adopted as follows: light red for heat release, light brown for smoke release, and light green for mass loss rate. A yellow fill color was used for the superposition plots.

## Results & Discussion

### ATH filled formulations, #1 through #6 (Table I)

Figure 1 shows the heat release rate (HRR) curves as a function of time versus ATH loading. All curves consist of two peaks with a valley between. Specifically the peak HRR is located on the second peak of each HRR curve and decreases from 343 kW/m<sup>2</sup> to 179 kW/m<sup>2</sup> as ATH loading increases. Generally when moving from 150 to 400 phr, the HRR line shapes become flatter (less intensity) and increasingly elongated (longer time). It is interesting to note that the ratio of the second peak height to the first peak height increases smoothly from 1.2 (150 phr) to 1.91 (350 phr). At 400 phr this trend reverses. The time to ignition, the first point where the HRR curve lifts above the x-axis, increases with increasing ATH loading (see Table I).

The peak HRR and average HRR (Figure 2) at the three heat flux levels, 35 kW/m<sup>2</sup>, 50 kW/m<sup>2</sup>, and 75 kW/m<sup>2</sup> are shown to be decreasing as a function of ATH loading which confirms the visual observation of the curves of Figure 1 that the average HRRs are decreasing.

The rate of smoke production (RoSP) curves can be seen to decrease in Figure 4 as ATH loading increases. Their line shapes are similar to their HRR counterparts. However the dissimilarity is the initial rise of the curves from the x-axis. This “time to smolder” occurs much earlier in the RoSP curves than the HRR curves and at almost the same time for all the curves. The “smoldering time interval” increases in length with increasing ATH and after that, ends with an abrupt rise in RoSP. The increasing smoldering time also appears to be linked to the increase in time to ignition.

Confirming the decreasing area of the RoSP curves, the specific extinction area (SEA) of Figure 5, or quantity of smoke, decreases with increasing ATH. However the SEA changes very little at the three heat flux levels, 35 kW/m<sup>2</sup>, 50 kW/m<sup>2</sup>, and 75 kW/m<sup>2</sup>. In contrast in Figure 6 the avg. RoSP, as well as the intrinsic RoSP, vs. ATH phr does change significantly with heat flux. Obviously one would expect the change RoSP to be dependent on the intensity of the heat flux of the

combustion phase however what is not so obvious is that the SEA exhibits very little dependence. This is because the SEA is dependent on the efficiency of the combustion process which in turn is dependent on a relatively large concentration of hydroxyl radicals working to break down high molecular weight pyrolysis products to volatile, low molecular weight products.

In Figure 7 the mass loss rate (MLR) curves show visually that it is decreasing as ATH increases, i.e., ATH is controlling the MLR. Furthermore the MLR curves have different line shapes than their HRR and RoSP counterparts. Some important points:

1. Indeed unlike the HRR and RoSP curves the first peaks of the 150 phr, 200 phr, and the 250 phr curves are higher in value than their second peaks. For the 350 and 400 phr curves the first and second peak heights reverse.
2. All curves show mass loss occurring over a longer time interval,
  - a. than their HRR and RoSP counterparts.
  - b. with increasing ATH.

Figure 8, a plot of avg. HRR vs. avg. MLR, show a very good straight-line, relationship. This is interpreted that as the rate of pyrolysis (MLR) increases the HRR increases in a quantitative way and it follows that HRR is being controlled by ATH loading.

#### **CaCO<sub>3</sub>, CaCO<sub>3</sub>/DBDE and ATH/DBDE filled formulations, #7 through #11 (Table I)**

Formulations #7 and #8 assumes that CaCO<sub>3</sub> is a non FR compound that can be substituted on a mass basis for ATH. This assumption allows for the FR results to be comparable to the 250 phr ATH formulation #3.

Figure 9 are plots of HRR with time. The CaCO<sub>3</sub> based formulations have very different line shapes because they do not have any ATH present. Most notable difference is the higher peak HRR of the non flame retardant CaCO<sub>3</sub> formulation versus the DBDE/CaCO<sub>3</sub> formulation. Two very important similarities:

1. They have the same ignition time.

DBDE has no effect on ignition time because there must be combustion for DBDE to be active via HBr poisoning of the hydroxyl radical

2. Both curves consist of a single peak.

There is nothing present to control the rate of pyrolysis in either formulation. Therefore it is simply a function of the HRR and no complex behavior is observed such as the two peaks and valley configuration characteristic of ATH decomposition.

In general the DBDE/ATH formulations (#9-#11) give similar line shapes as their ATH counterparts because the HRR is being controlled by the rate of pyrolysis (see Figure 8). Other similarities are an increasing ignition time and the two peaks and valley configuration, but with three notable differences.

1. The ignition times are longer.

2. The two peak HRRs of each curve are lower.

3. The curves are more elongated over time.

These differences are clearly shown in Figure 10 for the DBDE/ATH and ATH 150 phr formulations.

Figure 11, a plot of peak HRR (left) and THR (right) shows these quantities (see Table I) are lower for the DBDE/ATH formulations versus their ATH counterparts. It is important to note that the CaCO<sub>3</sub> filled formulations follow these trend lines (assume 0 phr ATH) for the peak HRR but do not for the THR. This is because the THR is also a function of the SEA, or amount of smoke produced.

Smoke is unconsumed fuel, the result of incomplete combustion. Incomplete combustion has a large effect on the THR but not nearly as much on the HRR. HRR is largely function of the rate of pyrolysis (see Fig. 8), but THR is not. This is further substantiated by comparing the CaCO<sub>3</sub> formulations with and without DBDE. Note that the DBDE/CaCO<sub>3</sub> formulation gives a lower THR and also has the greater SEA (see Figure 13 "0" phr ATH).

Recall Figure 5, the reduction in SEA as function of increasing ATH, argues that when the rate of fuel generation is minimized (minimization of the rate of pyrolysis) then combustion occurs most efficiently. This is because the ratio of hydroxyl radical concentration to fuel concentration is highest and SEA is reduced. On the other hand, hydroxyl radical depletion via HBr (DBDE decomposition) works to produce inefficient combustion, i.e., smoke and carbon monoxide [6, 7]. The ambivalent conclusion is that for the lowest smoke generation (and minimal carbon monoxide) the total heat release (THR) is maximized but this effect can be mitigated by extending the THR over time.

The RoSP curves are shown in Fig. 12. All curves are similar in shape to their HRR counterparts insofar that the CaCO<sub>3</sub> and DBDE/CaCO<sub>3</sub> curves consist of a single peak whereas the ATH/DBDE curves exhibit the two peaks and valley configuration of the ATH formulations which are also shown for comparison. The DBDE/CaCO<sub>3</sub> curve is highest in smoke production rate and as expected higher than its CaCO<sub>3</sub> comparison curve. However unexpectedly, at 350 phr ATH loading the ATH/DBDE has a lower peak RoSP than its ATH counterpart!

This behavior is confirmed in the double plots of Figure 13 where both SEA (left axis) and RoSP (right axis) are plotted as a function of ATH phr. The effect of ATH on DBDE for decreasing RoSP is dramatic. Both the SEA and avg. RoSP display a rapid decrease as ATH phr increases due to greater slopes of the DBDE/ATH lines versus their comparison ATH lines. The greater slopes gives intersections at about 350-370 phr. This surprising result, DBDE is found to help reduce SEA and RoSP at high ATH loadings, can be traced to the reduced HRR of the DBDE/ATH formulas versus their ATH counterparts.

The avg. MLR is shown in Figure 14. Two important differences are evident.

1. The MLR of the CaCO<sub>3</sub> formulas have a longer "time to mass loss" and accelerate much more rapidly to a single peak.
2. The ATH/DBDE curves are flatter and more elongated than their ATH counterparts.

Indeed the DBDE/ATH 350 phr is beginning to lose definition of its two peaks and valley. These important differences are clearly shown in Figure 15.

### Superposition of HRR, MLR and RoSP Curves

Figures 16, 17, and 18 are superpositions of the three important curves, MLR, HRR, and RoSP for DBDE/CaCO<sub>3</sub>, ATH, and DBDE/ATH formulas at the 250 phr loading. This allows one to understand the FR behavior of the composite as a sequence of events that is consistent with the FR mechanisms outlined in the Background section above.

First the simplest curve, Figure 16, the DBDE/CaCO<sub>3</sub> formulation is examined.

1. The external flux heats the composite's surface to the pyrolysis temperature, the organics begin to depolymerize, reach the flashpoint temperature in the flame zone and ignition occurs.

The time to ignition (initial HRR curve's rise from the x-axis) occurs before the time to mass loss (initial rise in the MLR curve). Unlike the ATH containing formulations the mass loss is completely due to pyrolysis of the organics.

2. The HRR rises rapidly to a peak which coincides with peaks in the MLR and RoSP.

The DBDE is reducing the HRR peak by interfering with the combustion process (Fig. 9) however there is nothing to prevent the pyrolysis reaction from slowing and the MLR rises to a peak at the about the same time as the HRR. A very high RoSP results from the flame zone being flooded with fuel coupled with an inefficient combustion process via the presence of HBr (see step 5 of the mechanism). Indeed the RoSP is higher for DBDE/CaCO<sub>3</sub> than the CaCO<sub>3</sub> formulation (see Fig. 12) because of hydroxyl radical poisoning.

3. After reaching their peaks all three curves decrease rapidly.

With all organics rapidly consumed the combustion process comes to an end.

Next, Figure 17, the 250 phr ATH formulation is examined.

1. The composite surface is heated by the external heat flux to the decomposition temperature of ATH, ~220° C. and an increase in the MLR curve observed.

The time to mass loss occurs before the time to ignition. This is in contrast to the behavior of DBDE/CaCO<sub>3</sub> of Figure 16 where the ignition occurs first. This is also shown in Figure 15 where the time to mass loss is shorter for the ATH containing formulas than that for

the CaCO<sub>3</sub> formulations. This initial mass loss is the result of HOH evolution. The HOH evolution is endothermic, cooling the composite's surface and preventing combustion.

2. The RoSP curve lifts off the x-axis and smoldering begins.
3. The RoSP plateau is indicative of continued smoldering. The MLR curve also begins to increase again but at a lower rate than initially.

The RoSP plateau, or smoldering, is observed because the ATH at the surface is depleted and the composite's surface temperature increases to the polymer's pyrolysis temperature. The ATH in the underlying surface layer decomposes endothermically creating a temporary steady state that delays ignition. The MLR increase at this point is composed of two variables, both ATH and polymer depolymerization.

4. Combustion begins when the HRR curve lifts off the x-axis.

When ATH depletion is essentially 100% complete on the surface and the adjacent underlying layer, then the volatile organics reach the flash point temperature and concentration necessary for combustion. This step determines time to ignition.

5. The HRR curve accelerates rapidly to a peak which is followed by the MLR curve and then the RoSP curve peaking.

HRR control of the combustion process at this step is proven by the occurrence of the HRR curve peaking first before the MLR and the RoSP peaks. The external heat flux of 50 kW/m<sup>2</sup>, becomes secondary because the 1<sup>st</sup> peak HRR is much greater at about 170 kW/m<sup>2</sup>.

6. The HRR curve decreases forming a valley between two peaks.

The valley, a period of equilibrium, is created by ATH decomposition causing the rate of pyrolysis to come into balance with the HRR, i.e., a stable feedback loop of fuel/heat production. Specifically this ATH, located deeper beneath the composite's surface, works to lower the rate of pyrolysis, and thereby equilibrates the HRR to a lower rate. Closer inspection shows this to be near the avg. HRR of 147 kW/m<sup>2</sup>. During this steady state interval it is important to note that the RoSP at 5 1/s is being suppressed by the steady rate of pyrolysis which is ultimately controlled by the ATH decomposition reaction.

7. After a period of relative steady state combustion the HRR accelerates to a 2<sup>nd</sup> peak higher than the first, which again is followed by the MLR and then the RoSP.

All the ATH is depleted and loss of the endothermic decomposition process results in a rapid internal temperature increase. In response the rate of pyrolysis increases resulting in rapid consumption of the remaining organic phase and the flooding of the flame zone with fuel.

The rapid increase in HRR results in its peak HRR of 252 kW/m<sup>2</sup>. This is accompanied by a rapid increase in both MLR (which at this point consists solely of fuel volatilization) and then RoSP. The interesting conclusion here is that the peak HRR decreases with ATH loading because the remaining amount of organic phase also decreases with ATH loading at the ATH total depletion point (see Figures 1, 2 & 9).

The complete depletion of the ATH is further proven by the rapid increase in RoSP. Indeed the loss of smoke suppression via loss of the ATH controlling the rate of pyrolysis, results in the RoSP increasing by greater than 2x, reaching its highest value of 12 l/s. The RoSP increases because the rapid influx of high molecular weight organic compounds overwhelms the hydroxyl radical decomposition reaction that produces low molecular weight volatile organics. As stated above, low molecular weight organics are necessary for the rapid, efficient combustion that produce very little smoke.

In this light the RoSP can be seen as a gauge for how efficient the combustion process is. This is an important consideration in explaining why the halogen FR mechanism is responsible for the increase in RoSP (see Step 5 of the halogen FR mechanism).

Figure 18, very similar to Figure 17 is indicative of the dominating effect the rate of pyrolysis (via ATH loading) has on all aspects of the burning process. However a significant difference, the addition of DBDE lowers the HRR by reducing the efficiency of the combustion process. The reduced HRR in turn reduces the heat in the feedback loop flowing back into the composite. This has the beneficial effect of reducing the rate of ATH decomposition. Furthermore the reduced HRR has a cumulative effect in the sense that the depletion of ATH occurs at a slower rate which in turn increases the time the rate of pyrolysis is minimized. This is why increased flattening (reduced intensity) and elongation (longer time) of the MLR, RoSP and HRR curves is observed as being more pronounced in the DBDE/ATH curves versus the ATH curves (see Figure 10). Another manifestation of this result is the decrease in RoSP and SEA in the discussion of Figure 13.

## Conclusions

1. Cone calorimeter is capable of generating data that gives a detailed insight into the FR mechanisms of FR active compounds.
2. DBDE can enhance the FR effect of ATH via reducing the HRR of the combustion phase thereby extending the lifetime of the ATH during the burn. At high ATH loading levels this results in increased smoke suppression.
3. Smoke suppression characteristic of the ATH SEA is related to the minimization of the heat release rate which in turn is a function of the rate of pyrolysis.

4. Superposition of the MLR, HRR, and RoSP curves can be interpreted to give a detailed sequence of an FR mechanism.
5. The occurrence of the second and highest peak in the heat release rate curve is the result of the 100% depletion of the ATH.

## References

1. Commission of the European Communities, Annex to the Directive 2002/95/EC, Official Journal of the European Union, L 271/48.
2. Website for RoHS UK : <http://www.rohs.gov.uk/content.aspx?id=12>  
Annulment of the Annex to the Directive 2002/95/EC, C116/2.
3. Challenger, P., "Halogen-Free Flame Retardant Thermoplastics", 2<sup>nd</sup> International Conference on Flame Retardants '85.
6. Rex, G. C. "Flame Retardant Performance of Halogen Free, Alumina Trihydrate Based Bulk Molding Compound", Composites 2006 Convention and Trade Show American Composites Manufacturers Association, October 18-20, 2006.
7. Rex, G.C., "Flame Retardant Performance of Halogen Free, Alumina Trihydrate Based Bulk Molding Compound", Fire & Materials 2007, Interscience Communications, UK, January 29-31, 2007.
8. Website for Custom Scientific Instruments Inc., Cone Calorimeter, <http://www.csi-instruments.com/>

## Biography

G. C. Rex

G.C. Rex has been the recipient of a B. S. degree in Chemistry (1973) from Bowling Green State University, an M.S. degree (1982) and a Ph. D. in Macromolecular Science (1989) from the University of Detroit. He was an analytical chemist at Allied Chemical from 1973-1976, an R&D chemist at Composite Technology from 1976-1982, a Sr. Research scientist at Union Carbide Corp. from 1986-2001, and Technology Leader at Dow Chemical from 2001-2003. Currently he is Thermoset Manager at J. M. Huber's Fairmount GA Technical Center.

**Table I  
BMC Formulas and Results**

	100% ATH						CaCO <sub>3</sub>	CaCO <sub>3</sub> & DBDE	ATH & DBDE		
	#1	#2	#3	#4	#5	#6			#7	#8	#9
NPG Isophthalic Polyester	80						80		80		
Saturated Polyester	15						15		15		
styrene	5						5		5		
t-butyl perbenzoate	1						1		1		
Viscosity reducer	1						1		1		
Zn St	1						1		1		
Stearic acid	2						2		2		
Alumina trihydrate	150	200	250	300	350	400	---	---	150	250	350
Ground Calcium Carbonate	---	---	---	---	---	---	250	250	---	---	---
Deca-BDE	---	---	---	---	---	---	---	10	10		
Antimony trioxide	---	---	---	---	---	---	---	2	2		
38% Mg(OH) <sub>2</sub> dispersion	3	2.7	2.3	2	1.7	1.4	2.3	2.3	2.8	2.3	1.7
1/4" chopped fiberglass	15% by wt.										
	Cone Calorimeter Results										
Time to Sustained Ignition, s	64	75	86	100	113	119	47	49	74	102	120
Time of Peak RHR, s	128	158	173	175	193	198	68	65	170	203	250
Peak Rate of Heat Release, kW/m <sup>2</sup>	343	280	252	252	233	179	477	379	255	237	169
Avg. HRR (35 kW/m <sup>2</sup> )	181	153	126	112	95	83	---	---	---	---	---
Avg. HRR (50 kW/m <sup>2</sup> )	194	166	147	135	117	100	268	202	165	128	98.2
Avg. HRR (75 kW/m <sup>2</sup> )	203	182	158	150	128	109	---	---	---	---	---
Intrinsic HRR	165	129	103	84	71	63	---	---	---	---	---
Total Heat Released, MJ/m <sup>2</sup>	31.5	31.3	27.0	24.7	22.0	20.8	27.4	20.6	27.9	23.5	20.8
Avg. Heat of Combustion, MJ/kg	15.8	14.7	13.3	12.8	11.1	10.9	24.2	17.7	12.2	10.7	10.1
Avg. MLR (35 kW/m <sup>2</sup> )	9.8	8.8	8.1	7.2	6.6	6.1	---	---	---	---	---
Avg. MLR (50 kW/m <sup>2</sup> )	11.6	10.7	9.8	9.4	8.9	8.1	---	---	---	---	---
Avg. MLR (75 kW/m <sup>2</sup> )	15.2	14.1	13.5	12.9	12.2	11.5	---	---	---	---	---
Intrinsic MLR	5.0	4.1	3.2	2.2	1.8	1.4	---	---	---	---	---
Avg. RoSP (35 kW/m <sup>2</sup> )	7.9	5.5	4.3	3.2	2.3	1.7	---	---	---	---	---
Avg. RoSP (50 kW/m <sup>2</sup> )	8.2	5.9	4.9	4.4	3.3	2.3	13.7	18.7	12.8	6.9	2.8
Avg. RoSP (75 kW/m <sup>2</sup> )	9.4	7.3	5.8	5.0	3.8	2.5	---	---	---	---	---
Intrinsic RoSP	6.4	3.8	3.0	2.1	1.5	1.2	---	---	---	---	---
Avg. Sp. Extinction Area, m <sup>2</sup> /kg	541	446	371	343	277	202	1033	1462	899	573	306
Time of Peak SEA, s	160	175	190	190	298	213	63	50	183	210	265

